Dirac light bullets in nonlinear binary waveguide arrays

Truong X. Tran, and Dũng C. Duong

Citation: Chaos **28**, 013112 (2018);
View online: https://doi.org/10.1063/1.4985098
View Table of Contents: http://aip.scitation.org/toc/cha/28/1
Published by the American Institute of Physics

Dirac light bullets in nonlinear binary waveguide arrays

Truong X. Tran and Dũng C. Duong
Department of Physics, Le Quy Don University, 236 Hoang Quoc Viet Str., 10000 Hanoi, Vietnam

(Received 25 May 2017; accepted 28 December 2017; published online 11 January 2018)

We investigate the formation and dynamics of spatially broad Dirac light bullets in nonlinear binary waveguide arrays. We show that a Dirac light bullet can be formed during propagation when a pulse with an initial profile slightly different from the one of the Dirac light bullet is launched into the system. We also reveal that these Dirac light bullets are metastable and can propagate without significant distortion for hundreds of dispersion lengths even in the presence of the Raman effect, group velocity mismatch, and group velocity dispersion difference between adjacent waveguides. *Published by AIP Publishing*. https://doi.org/10.1063/1.4985098

Discrete gap solitons in binary waveguide arrays (BWAs) have been intensively investigated both theoretically and experimentally. Recently, these solitons have been demonstrated to be optical analogues of Dirac solitons (DS) in a nonlinear extension of the relativistic Dirac equation. Up to now, all these Dirac solitons have been studied in the continuous-wave (CW) regime when a beam is launched into binary waveguide arrays to form a spatial Dirac soliton. In this work, we investigate the formation and dynamics of Dirac light bullets (DLBs) in binary waveguide arrays with both Raman and Kerr nonlinearities, where a pulse is used to form spatiotemporal localized structures. We show that broad Dirac light bullets are metastable and can propagate robustly for significant lengths even under the influence of temporal effects such as the Raman nonlinearity, group velocity mismatch, and group velocity dispersion (GVD) difference between adjacent waveguides in binary waveguide arrays.

I. INTRODUCTION

Waveguide arrays (WAs) have been exploited to investigate various fundamental photonic phenomena such as discrete diffraction and [1,2] discrete solitons.[1,3,4] Discrete solitons in 2D lattices of nonlinear waveguides can potentially be used in all-optical integrated circuits.[5] Recently, it was shown that most of the nonlinear phenomena usually associated to fiber optics, for instance, the emission of resonant radiation from solitons and soliton self-wavenumber shift can also occur in Was,[6,7] and the supercontinuum in both frequency and wave number can be generated in Was.[8]

Waveguide arrays have also been exploited to mimic the evolution of a non-relativistic quantum mechanical particle in a periodic potential.[9] Many fundamental phenomena in non-relativistic quantum mechanics such as Bloch oscillations[1,9,10] and Zener tunneling[11,12] have been simulated and demonstrated by using WAs. However, in order to simulate phenomena in relativistic quantum mechanics, one needs to use binary waveguide arrays (BWAs) instead of conventional WAs. For example, Klein tunneling,[13,14] *Zitterbewegung*,[15,16] and fermion pair production,[17] which all emerge from the Dirac equation,[18] have been simulated with BWAs. The discrete gap solitons in the classical context have been found in BWAs.[19–22] Gap, out-gap solitons, and breathers in BWAs have also been investigated in Refs. 23 and 24. These gap solitons were already studied for diatomic lattices in 1992.[25] In 2014, the explicit suggestion to exploit BWAs for simulating the quantum nonlinear Dirac equation was put forward in Ref. 26, where the gap solitons in BWAs, for the first time, have been demonstrated to be optical analogues of Dirac solitons (DSs) emerging from the relativistic nonlinear Dirac equation. The stability, dynamics, and different scenarios of DS interaction have been analyzed in Ref. 27. The properties of 2D DSs in square binary waveguide lattices have been investigated in Ref. 28. The higher-order Dirac solitons in BWAs have been studied in Ref. 29. Note that the nonlinear Dirac equations have been investigated since a long time, for instance, by Heisenberg.[30] Nonlinear Dirac equations have also been exploited in atomic, nuclear, and gravitational physics.[31–34]

The concept of gap solitons, or more proper solitary waves, in nonlinear optics, was introduced for the first time in superlattices in 1987.[35] Later, gap solitons have been intensively studied in fiber Bragg gratings (FBGs) and other periodic structures.[4] In 1989, slow gap solitons in FBGs were predicted in Ref. 36, and the gap soliton solution of the coupled-mode equations in FBGs was obtained in Ref. 37 via a transformation of the soliton supported by the massive Thirring model in the relativistic quantum field theory.[38] It has also been shown that under certain conditions, the coupled-mode equations in fiber Bragg gratings can be transformed into the nonlinear Schrödinger equation.[39] The bifurcation of gap solitons in FBGs has been analyzed in Ref. 40, where the existence diagram for various types of gap solitons in FBGs has been shown. The stability of gap solitons has been investigated in Refs. 41 and 42. The first experimental observation of gap solitons in FBGs has been reported in Ref. 43. A brief survey of studies on gap solitons in FBGs has been given in Ref. 44.

Light bullets (LBs)—solitary waves localized in both time and space—can propagate without distortion due to the combination of the diffraction, anomalous dispersion, and nonlinearity.[45,46] They have been intensively explored in both conservative[4,47–53] and dissipative systems.[54–56] In

conservative bulk media with Kerr nonlinearity, LBs are known to be unstable and a collapse always happens.[4,45] However, the discrete nature of WAs is able to stop the collapse.[47] Therefore, nonlinear WAs present an interesting system to study LBs.[47–53] Recently, it has been shown in Ref. 57 that broad LBs can be established during propagation in nonlinear conventional WAs (consisting of identical waveguides) even in the presence of disturbing factors such as the Raman effect, higher-order dispersion (HOD), and wavelength dependence of the coupling coefficient between adjacent waveguides (further referred to as the coupling dispersion). Dynamics of optical gap-soliton bullets in a waveguide grating (i.e., a planar waveguide with a Bragg grating in the direction of propagation) has been investigated in Ref. 58. Light bullets in Ref. 58 are bullets of the so-called $(2+1)$D case, where they are confined simultaneously in time, in one transverse direction (x), and in the propagation direction z (not counting the other transverse direction (y) where the planar waveguide mode is always confined). The frequency of these light bullets lies within the band-gap of the structure, therefore, they are also called gap-soliton bullets. The existence of both stationary and travelling gap-solitons bullets and their trapping at localized defects in waveguide gratings has been investigated in detail in Ref. 59. The formation of gap-soliton bullets propagating with slow group velocities in WAs with phase-shifted Bragg gratings has been experimentally demonstrated in Ref. 60. Gap-soliton bullets in photonic crystals with a two-dimensional (2D) square and triangular symmetry group, as well as a 3D fcc symmetry group have been investigated in great detail in Ref. 61.

So far, all above-mentioned Dirac solitons have been studied in the continuous-wave (CW) regime, i.e., when a beam is launched into BWAs to form a spatial Dirac soliton. In this paper, we aim to investigate the formation and dynamics of Dirac light bullets (further referred to as DLBs) in BWAs where a pulse is used. To the best of our knowledge, this is the first time that DLBs have ever been studied. We first present the generalized coupled-mode equations (GCMEs) governing the spatiotemporal evolution of pulses in BWAs with Kerr nonlinearity and Raman effect. Then, we explore the generation of broad DLBs and their dynamics during propagation. We demonstrate that these DLBs are metastable and can propagate without significant distortion for significant lengths even in the presence of the temporal effects.

The remainder of this paper is organized as follows: in Sec. II, the set of generalized coupled-mode equations governing pulse propagation in BWAs is derived. Subsequently, in Sec. III, we investigate the formation and dynamics of broad DLBs in BWAs where a simplified model of equations is used. In Sec. IV, we study the influence of disturbing factors on the generation and dynamics of DLBs. Finally, in Sec. V, we summarize the findings of this work.

II. GENERALIZED COUPLED-MODE EQUATIONS

Our starting point is the generalized coupled-mode equations (GCMEs) in the frequency domain governing a pulse propagation in a BWA composed by two interleaved types of waveguides made of silica [see also Eqs. (2.1.4) and (2.1.5) in Ref. 62]

$$\frac{d\tilde{A}_n}{dz} = i\left[\beta^{(n)}(\omega) + \Delta\beta_{NL}^{(n)} - \beta_0)\right]\tilde{A}_n + i\kappa(\omega)\left[\tilde{A}_{n+1} + \tilde{A}_{n-1}\right], \tag{1}$$

where $\tilde{A}_n$ is the electric field envelope in the n-th waveguide in the frequency domain, z is the longitudinal coordinate, $\beta^{(n)}(\omega)$ is the mode-propagation constant of the n-th waveguide at the frequency ω, $\Delta\beta_{NL}^{(n)}$ is the nonlinear contribution to the mode-propagation constant in the n-th waveguide, β_0 is the average value of the mode-propagation constants at the carrier frequency ω_0 for two different types of waveguides in BWAs, and $\kappa(\omega)$ is the frequency-dependent coupling coefficient between identical adjacent waveguides. Note that in most cases, the coupling coefficient κ is often treated as a constant, but in general, it also depends on the frequency.[8,57]

The above frequency-domain GCMEs can be converted to the time domain by expanding both $\beta(\omega)$ and $\kappa(\omega)$ in the Taylor series around ω_0, replacing $(\omega-\omega_0)$ by a time derivative while taking the inverse Fourier transform. In doing so, we obtain the following GCMEs in the time domain:

$$\left\{i\partial_z + \sum_{m\geq 1}\frac{\beta_m^{(2n)}}{m!}(i\partial_t)^m - \delta_a\right\}A_{2n} + \kappa(i\partial_t)[A_{2n+1}+A_{2n-1}] + \gamma^{(2n)}\left(1+\frac{i}{\omega_0}\partial_t\right)A_{2n}(z,t)\int_{-\infty}^{\infty}R(t')|A_{2n}(z,t-t')|^2dt' = 0, \tag{2}$$

$$\left\{i\partial_z + \sum_{m\geq 1}\frac{\beta_m^{(2n+1)}}{m!}(i\partial_t)^m + \delta_a\right\}A_{2n+1} + \kappa(i\partial_t)[A_{2n+2}+A_{2n}] + \gamma^{(2n+1)}\left(1+\frac{i}{\omega_0}\partial_t\right)A_{2n+1}\int_{-\infty}^{\infty}R(t')|A_{2n+1}(z,t-t')|^2dt' = 0, \tag{3}$$

where $\beta_m^{(q)}$ is the standard m-th order group velocity dispersion (GVD) coefficient of the q-th waveguide ($q=2n$, $2n+1,\ldots$). Note that the group velocity at ω_0 in the q-th waveguide $v_g^{(q)}(\omega_0) = 1/\beta_1^{(q)}(\omega_0)$. The propagation mismatch is defined as follows: $\delta_a = [\beta^{(2n+1)}(\omega_0) - \beta^{(2n)}(\omega_0)]/2$, which represents the binary nature of the system and is due to the fact that two adjacent waveguides in BWAs are asymmetric. Meanwhile, the operator for the coupling coefficient is given by $\kappa(i\partial_t) \equiv \sum_{m\geq 0}\frac{\kappa_m}{m!}[i\partial_t]^m$ and κ_m is the m-th order derivative of $\kappa(\omega)$ at ω_0. The standard nonlinear parameter for the q-th waveguide is denoted via $\gamma^{(q)}$. The nonlinear response function $R(t) = (1-f_R)\delta(t) + f_R h_R(t)$, where the first term represents the instantaneous electronic contribution with $\delta(t)$ being the Dirac delta function, $h_R(t)$ is the Raman response function of the core, and f_R represents its fractional contribution.[63] For silica, $f_R \simeq 0.18$ and the Raman effect is included through a simple model in which $h_R(t)$ has the form $h_R(t) = \frac{\tau_1^2+\tau_2^2}{\tau_1\tau_2^2}\exp(-t/\tau_2)\sin(t/\tau_1)\Theta(t)$, where $\tau_1 = 12.2$ fs and $\tau_2 = 32$ fs, and $\Theta(t)$ is the Heaviside step function that ensures causality.[63] The self-steepening

effect is included through the derivative ∂_t in the nonlinear terms. Now, we introduce dimensionless variables $\xi = z/L_D^{(2n)}$, $\tau = (t - z\beta_1^{(2n)})/T_0$, and $a_n = A_n/\sqrt{P_0}$, where $L_D^{(2n)} = T_0^2/|\beta_2^{(2n)}(\omega_0)|$ is the dispersion length of even waveguides and T_0 is the time scale of the pulse duration. The power scale is $P_0 = 1/[\gamma^{(2n)} L_D^{(2n)}]$. All these scales for normalization are standard in the case of a single optical fiber.[63] With these new variables, Eqs. (2) and (3) are equivalent to the following dimensionless GCMEs:

$$\begin{aligned} &i\partial_\xi a_{2n}(\xi,\tau) + D^{(2n)}(i\partial_\tau)a_{2n} \\ &\quad -\sigma a_{2n} + L_D^{(2n)}\kappa(i\partial_\tau)[a_{2n+1} + a_{2n-1}] \\ &\quad + \left(1 + \frac{i\partial_\tau}{\omega_0 T_0}\right) a_{2n} \int_{-\infty}^{\infty} r(\tau')|a_{2n}(\xi, \tau - \tau')|^2 d\tau' = 0, \quad (4) \\ &i\partial_\xi a_{2n+1}(\xi,\tau) + id_g\partial_\tau a_{2n+1} + d_2 D^{(2n+1)}(i\partial_\tau)a_{2n+1} \\ &\quad +\sigma a_{2n+1} + L_D^{(2n)}\kappa(i\partial_\tau)[a_{2n+2} + a_{2n}] \\ &\quad + d_{NL}\left(1 + \frac{i\partial_\tau}{\omega_0 T_0}\right) a_{2n+1} \int_{-\infty}^{\infty} r(\tau')|a_{2n+1}(\xi, \tau - \tau')|^2 d\tau' = 0, \end{aligned} \quad (5)$$

where the dispersion operators have the standard form $D^{(q)}(i\partial_\tau) \equiv \frac{1}{2}s^{(q)}\partial_\tau^2 + \sum_{m\geq 3}\alpha_m^{(q)}[i\partial_\tau]^m$ for each q-th waveguide with $s^{(q)} = +1$ (-1) for anomalous (normal) GVD regime, and coefficients $\alpha_m^{(q)} \equiv \beta_m^{(q)}/[m!|\beta_2^{(q)}|T_0^{m-2}]$. Meanwhile, the operator for the coupling coefficient has the form $\kappa(i\partial_\tau) \equiv \sum_{m\geq 0}\frac{\kappa_m}{m!T_0^m}[i\partial_\tau]^m$, and the dimensionless function $r(\tau)$ is obtained by rescaling time t with T_0 in the response function $R(t)$. In Eqs. (4) and (5), we have introduced four dimensionless parameters related to the asymmetric nature of the two adjacent waveguides in BWAs: $\sigma = \delta_a L_D^{(2n)}$, $d_g = L_D^{(2n)}[\beta_1^{(2n+1)} - \beta_1^{(2n)}]/T_0$, $d_2 = \beta_2^{(2n+1)}/\beta_2^{(2n)}$, and $d_{NL} = \gamma^{(2n+1)}/\gamma^{(2n)}$. Physically, σ and d_g represent, respectively, phase- and group-velocity mismatch, whereas d_2 and d_{NL} take into account differences in group velocity dispersion and nonlinear properties, respectively, between adjacent waveguides in BWAs. To some extent, Eqs. (4) and (5) are similar to Eqs. (2.4.1) and (2.4.2) for asymmetric couplers (which consist of just two different waveguides) in Ref. 62. However, there are several differences between Eqs. (2.4.1) and (2.4.2) in Ref. 62 and Eqs. (4) and (5) in our work. First, Eqs. (2.4.1) and (2.4.2) in Ref. 62 deal with just two asymmetric waveguides, whereas Eqs. (4) and (5) cope with many waveguides in BWAs, thus the coupling terms between these equations are obviously different. Second, Eqs. (2.4.1) and (2.4.2) in Ref. 62 are limited to the second-order dispersion and the coupling coefficient is treated constant for the whole spectrum of the pulse, whereas in Eqs. (4) and (5), we use the full dispersion for each waveguide and the coupling coefficient is frequency-dependent in the form of the operator $\kappa(i\partial_\tau)$. Third, Eqs. (2.4.1) and (2.4.2) in Ref. 62 take into account just the Kerr nonlinearity, whereas Eqs. (4) and (5) deal with both Raman and Kerr nonlinearities and also the self-steepening term. To the best of our knowledge, all previous analytical studies dealing with BWAs are just limited to the CW regime, thus, Eqs. (4) and (5) which govern the pulse propagation process in BWAs are derived here for the first time in the most general form for waveguides with Kerr and Raman nonlinearities. Although two adjacent waveguides in BWAs are asymmetric, therefore, their nonlinear coefficients are different which means $d_{NL} \neq 1$ in the general case. However, to simplify the analysis in BWAs, the nonlinear coefficients are often considered identical, thus, $d_{NL} = 1$.[19,26] This approximation is reasonable because, as pointed out in Ref. 26, one of the Dirac soliton components (for instance, the odd component a_{2n+1}) is very weak, thus, the nonlinear term associated with this weak component in Eq. (5) plays a minor role, and from now on in this work we also will set $d_{NL} = 1$. However, Eqs. (4) and (5) are still very complicated, in order to investigate the formation, dynamics of the DLBs in BWAs, and the influence of many disturbing factors on DLBs in Secs. III and IV Eqs. (4) and (5) will be used with some further simplifications.

III. BROAD DIRAC LIGHT BULLET GENERATION AND ITS DYNAMICS IN A SIMPLIFIED MODEL

In this section, we analyze the generation of spatially broad DLBs in BWAs in the anomalous GVD regime in a simplified model where HOD, the coupling dispersion, the self-steepening effect, and the Raman effect are excluded. At the beginning, we also ignore the group velocity mismatch and group velocity dispersion difference between two adjacent waveguides, i.e., we set $d_g = 0$ and $d_2 = 1$. In this case, Eqs. (4) and (5) are much simplified as follows:

$$i\partial_\xi a_n + \frac{1}{2}\partial_\tau^2 a_n + \frac{1}{2}\eta[a_{n+1} + a_{n-1}] - (-1)^n\sigma a_n + |a_n|^2 a_n = 0, \quad (6)$$

with $\eta = 2L_D^{(2n)}\kappa(\omega_0)$. In the CW regime, the second-order derivative in Eq. (6) is eliminated and we obtain the standard coupled-mode equations for beams in BWAs[19,26] from which the Dirac solitons solutions are found.[26] Now, we write Eq. (6) in the form

$$\begin{aligned} &i\partial_\xi a_n + \frac{1}{2}\partial_\tau^2 a_n + \frac{1}{2}\eta[a_{n+1} - 2a_n + a_{n-1}] + \eta a_n \\ &\quad -(-1)^n\sigma a_n + |a_n|^2 a_n = 0, \end{aligned} \quad (7)$$

and eliminate the linear term ηa_n by using the transformation $a_n' = a_n \exp(i\eta\xi)$. By doing so, we get the following equation in the continuum limit:

$$i\partial_\xi a_n + \frac{1}{2}\partial_\tau^2 a_n + \frac{1}{2}\eta\partial_n^2 a_n - (-1)^n\sigma a_n + |a_n|^2 a_n = 0. \quad (8)$$

For making notations simple, we drop the prime symbol in superscripts in Eq. (8). If the factor $\eta \neq 1$, one can always use the rescaling technics by putting the variable $n = \sqrt{\eta}m$ in Eq. (8) such that its counterpart in the new equation is equal to unity. Thus, below the factor η will be set equal to unity. Without the binary term represented by the coefficient σ, Eq. (8) would be completely identical to Eq. (5) in Ref. 57 where LBs in conventional WAs consisting of identical waveguides are investigated. As pointed out in Ref. 57,

if $\eta = 1$, the transverse profile of broad LBs in conventional WAs depends on the variable $\rho = \sqrt{\tau^2 + n^2}$. In what follows, we show the generation of broad DLBs by using the following initial condition at the BWA input for simulating Eq. (6): $a_n(\tau, 0) = b_0 \mathrm{sech}(\tau/5) a_n^{DS}(z = 0)$, where the input peak amplitude b_0 will be changed to study the DLB generation, $a_n^{DS}(z = 0)$ is the Dirac soliton solution at the input (i.e., when $z = 0$), and $a_n^{DS}(z)$ is the Dirac soliton solution at any propagation distance z in the CW regime in the form of Eq. (6) in Ref. 26 as follows:

$$\begin{bmatrix} a_{2n}^{DS}(z) \\ a_{2n-1}^{DS}(z) \end{bmatrix} = \begin{bmatrix} i^{2n} \dfrac{\eta}{n_0\sqrt{\sigma}} \mathrm{sech}\left(\dfrac{2n}{n_0}\right) \\ i^{2n} \dfrac{\eta^2}{2n_0^2\sigma\sqrt{\sigma}} \mathrm{sech}\left(\dfrac{2n-1}{n_0}\right) \tanh\left(\dfrac{2n-1}{n_0}\right) \end{bmatrix} e^{izf}, \tag{9}$$

where the propagation constant parameter $f = -\sigma + (\eta^2/(2n_0^2\sigma))$ and n_0 characterizes the Dirac soliton width. As pointed out in Ref. 26, the Dirac soliton solution in the form of Eq. (9) is derived under the condition that $n_0|\sigma| \gg \eta$ which means $\eta^2/(2n_0^2|\sigma|) \ll |\sigma|/2$. As a result, we get the following important relation for the propagation constant parameter $|\sigma| > f > -|\sigma|$.

Before going further, we would like to show that the Dirac soliton solution in the form of Eq. (9) is indeed a gap soliton. In the CW and linear regime, Eq. (6) is much simplified and reduced to Eq. (1) in Ref. 16, where its linear dispersion relation has been analyzed and shown explicitly in Fig. 1(b) therein. Actually, the BWAs in the linear regime support two minibands, separated by a narrow gap of 2σ [see Fig. 1(b) in Ref. 16], defined by the following dispersion curves:

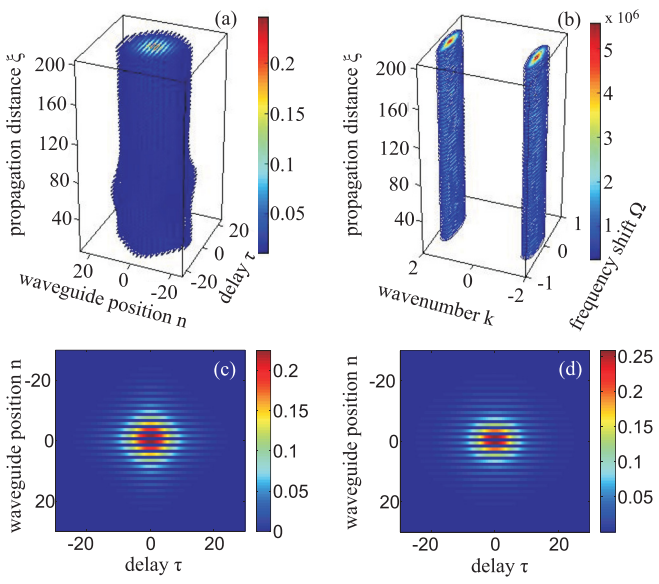

FIG. 1. (a) and (b) Generation of a broad Dirac light bullet in the (n,τ,ξ) and (k,Ω,ξ) spaces, respectively, when $b_0 = 1.26$. The first and last frames in (a) are shown in (c) and (d), respectively, in the (n,τ) plane. The parameters: $\sigma = 1.2$, $n_0 = 5$, $\eta = 1$, $d_2 = 1$, $d_g = 0$, the time scale $T_0 = 40$ fs, the length scale $L_D^{(2n)} = 3.56$ mm, and the power scale $P_0 = 2.8$ kW.

$$\omega_{\pm}(q) = \pm\sqrt{\sigma^2 + \eta^2 \cos^2(qd)}, \tag{10}$$

where $2d$ is the BWAs period in the transverse direction and q is the Bloch wave number. As explained above, we have $|\sigma| > f > -|\sigma|$, thus, now it is clear to see that the propagation constant parameter f of the Dirac soliton falls in the minigap of the BWAs. As a result, one can say, that the Dirac soliton solution in the form of Eq. (9) is a gap soliton as briefly explained in Ref. 26. From Eq. (10), as pointed out in Ref. 16, near $q = \pi/2d$, the dispersion curves of the two minibands form two opposite hyperbolas, and therefore mimic the typical hyperbolic energy-momentum dispersion relation for positive-energy and negative-energy branches of a freely moving relativistic massive particle. This suggests that light propagation in the BWAs for Bloch waves with wave number q close to $\pm\pi/2d$ (which corresponds to the normalized wave number $k \equiv qd = \pm\pi/2$, and the excitation under Bragg angles for input beams) simulates the temporal dynamics of the relativistic Dirac equation. The Dirac soliton solution in the form of Eq. (9) has two components of the normalized wave number also centered at $\pm\pi/2$ [see Fig. 2(b) in Ref. 26]. Thanks to that the nonlinear coupled-mode, Eq. (6) can be converted into the nonlinear relativistic 1 D Dirac equation in Ref. 26. It is worth noting that the well-known dispersion relationship in FBGs [see Eq. (5.2.18) and Fig. 5.2. in Ref. 4] also forms exactly two opposite hyperbolas. Therefore, the coupled-mode equations in FBGs can also be converted into the relativistic Dirac equation as explicitly shown in Ref. 64. This is not surprising, because, as mentioned in the Introduction, the gap soliton solution of the coupled-mode equations in FBGs was already obtained in 1989 via a transformation of the soliton supported by the massive Thirring model in the relativistic quantum field theory.[37] So, the gap solitons in FBGs discussed in the Introduction are also optical analogues of relativistic Dirac solitons, obviously.

For WAs consisting of just uniform waveguides (i.e., when $\sigma = 0$), within the coupled-mode approach, the linear dispersion of WAs is reduced to $\omega = \eta\cos(qd)$ [see Eq. (2.5) in Ref. 9]. This means the band structure in WAs consists of a single band embedded within two semi-infinite gaps (see Fig. 2.3 in Ref. 9). By using the Floquet-Bloch analysis in WAs—a more general approach[65]—one can get the band structure consisting of several bands separated by gaps (see Fig. 2.2 in Ref. 9). However, all these structures do not have anything similar to two opposite hyperbolas. Therefore, with WAs one cannot mimic the typical hyperbolic energy-momentum dispersion relation in 1 D Dirac equations. As a result, so far one can only convert coupled-mode equations in WAs into the Schrödinger equation, but not the Dirac one. Therefore, to the best of our knowledge, gap solitons in WAs have not been shown to be analogs of Dirac solitons.

The evolution of the pulse is illustrated in Fig. 1(a) in the (n,τ,ξ) space for the input peak amplitude $b_0 = 1.26$. The first and last frames of Fig. 1(a) are shown in the (n,τ) plane in Figs. 1(c) and 1(d), respectively. As demonstrated in Fig. 1(a), at the beginning the adjustment of the pulse profile takes place, then after reaching the propagation distance

$\xi \simeq 60$, the pulse acquires a stable profile, and propagates like a DLB without any significant distortion. As shown in Fig. 1(c), the input transversal profile of the pulse is similar to a square, especially in the pulse periphery. However, at the output [see Fig. 1(d)], as LBs in WAs consisting of identical waveguides [see Fig. 2(d) in Ref. 57], the established profile of the DLB is more reminiscent of a circle. Because the factor $\eta = 1$ in Fig. 1 and we obtain the DLB with circular profiles. Obviously, if $\eta \neq 1$, we will obtain DLBs with oval profiles. The distinguishing feature of DLBs is its binary nature where its strong component is located in one type of waveguides (with even position n in Fig. 1) and its weak component is located at the other type of waveguides (with odd position n in Fig. 1). Meanwhile, the LBs in the normal WA have a profile which is quite smooth across the WA.[57]

Now, if we perform the Fourier transform $a(n,\tau,\xi) \rightarrow \tilde{a}(k,\Omega,\xi)$ (time domain τ and space domain n are transformed into the frequency shift domain Ω and the transverse wavenumber domain k, respectively), then from Fig. 1(a) we get Fig. 1(b) showing the DLB evolution in the (k,Ω,ξ) space. As shown in Fig. 1(b), the profile of the established DLB in the (k, Ω) plane is also stable during propagation. It is worth emphasizing that although the input profile of the pulse is not exactly the one of the established DLB, nevertheless, during propagation the pulse will adjust and acquire the profile of the DLB. This shows that broad DLBs in BWAs can form spontaneously and are robust. To estimate the real physical parameters of the calculated DLB, we use typical parameters of BWAs reported in Ref. 16, where the coupling coefficient $\kappa = 0.14\,\mathrm{mm}^{-1}$ and the propagation mismatch $\delta_a = 0.336\,\mathrm{mm}^{-1}$. The time scale T_0 is set to be 40 fs, $\beta_2^{(2n)} = -0.45$ ps^2/m, and the nonlinear parameter $\gamma^{(2n)} = \gamma^{(2n+1)} = 0.1\ \mathrm{m}^{-1}\,\mathrm{W}^{-1}$. With these parameters, one can calculate that the dimensionless parameters $\sigma = 1.2$ and $\eta = 1$, the length scale $L_D^{(2n)} = 3.56\,\mathrm{mm}$, and the power scale $P_0 = 2.8\,\mathrm{kW}$ (thus, the peak power in Fig. 1 is around 175 W).

Now, we investigate two special sections of Fig. 1(a) along the ξ-axis. Figure 2(a) shows the section for the central waveguide with $n = 0$. Meanwhile, Fig. 2(b) shows the section for the central delay ($\tau = 0$). The common feature of pulse dynamics in both Figs. 2(a) and 2(b) is that at the initial stage, the pulse is slightly compressed in both τ and n, but from a propagation distance of about $\xi \simeq 60$ the established profile of the DLB becomes stable. The dashed red curve in Fig. 2(c) plots the input signal with the sech profile in Fig. 2(a) as a function of the delay τ, whereas the solid blue curve in Fig. 2(c) depicts the output profile in Fig. 2(a). Meanwhile, the red curve with round markers in Fig. 2(d) represents the input profile as a function of the waveguide position n in Fig. 2(b), whereas the blue curve with square markers in Fig. 2(d) represents the output profile in Fig. 2(b).

In Figs. 1 and 2, the input profile with $b_0 = 1.26$ is used and, as a result, a broad DLB is formed during propagation. Now, we change the peak amplitude of the initial pulse by 6% to investigate different scenarios of pulse dynamics in BWAs. If a pulse with lower input peak amplitudes is used, one can expect that now the diffraction-based broadening prevails over the nonlinearity-based focusing which will lead

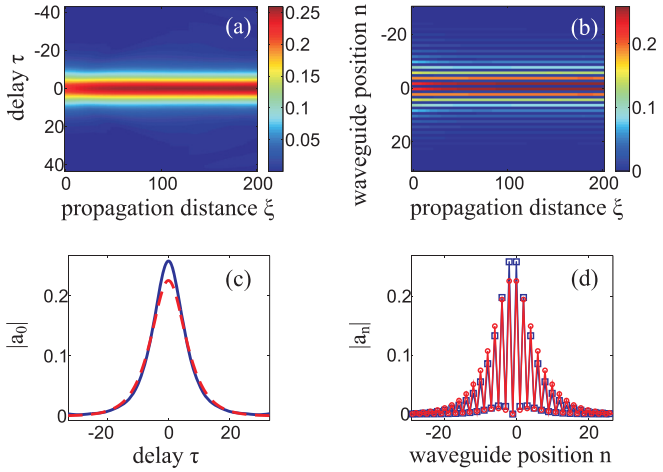

FIG. 2. (a) Pulse propagation in the central waveguide $n = 0$ and (b) and with the delay $\tau = 0$. (c) The dashed red curve plots the input sech profile as a function of the delay τ in the central waveguide $n = 0$, whereas the solid blue curve—output profile. (d) The red curve with round markers depicts the input profile as a function of the waveguide position n at the central delay $\tau = 0$, whereas the blue curve with square markers—output profile.

to the pulse spreading in both time and space. Indeed, this is confirmed in Fig. 3(a) with $b_0 = 1.185$. On the contrary, if input peak amplitudes are higher, the pulse focusing in both space and time can happen during propagation as clearly shown in Fig. 3(b) with $b_0 = 1.335$. After the compression in space and time at $\xi \simeq 100$, the pulse spreads out again. Obviously, the closer the input peak amplitude to the value $b_0 = 1.26$, the better the pulse will retain its profile during propagation as the DLB shown in Figs. 1 and 2.

IV. INFLUENCE OF DISTURBING FACTORS ON THE GENERATION AND DYNAMICS OF DIRAC LIGHT BULLETS

In Sec. III, the generation and dynamics of broad DLBs are studied by using a simplified model in the absence of several disturbing factors such as the group velocity mismatch, GVD difference, Raman effect, HOD, and coupling dispersion. All these effects can play some roles in pulses dynamics, in particular, for short pulses. Now, it is time for us to study the influence of some relevant disturbing factors on the generation and dynamics of DLBs in BWAs. With this aim, Eqs. (4) and (5) are used in this section instead of

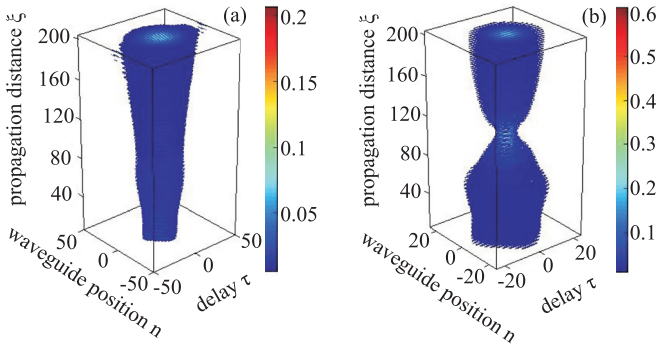

FIG. 3. (a) and (b) Evolution of a pulse in the (n,τ,ξ) space when $b_0 = 1.185$ and 1.335, respectively. All other parameters are the same as in Fig. 1.

Eq. (6) for the simplified model. However, as pointed out in Ref. 57, the influence of HOD and coupling dispersion is negligible for broad LBs. So, in this work, we neglect these two effects and for the rest of this work we set $L_D^{(2n)}\kappa(i\partial_\tau) = \eta/2 = 0.5$, and $D^{(q)}(i\partial_\tau) = \frac{1}{2}s^{(q)}\partial_\tau^2$ for Eqs. (4) and (5).

We first study the influence of the group velocity mismatch represented by the parameter d_g in Eqs. (4) and (5). In Figs. 4(a) and 4(b), we show the propagation of a pulse in the (n,τ,ξ) space when $d_g = 2$ and -2, respectively. All other parameters used in Fig. 4 are the same as in Fig. 1. Note that if $d_g > 0$, then we have $\beta_1^{(2n+1)} > \beta_1^{(2n)}$, thus the group velocity in odd waveguides is smaller than the one in even waveguides, i.e., $v_g^{(2n+1)} < v_g^{(2n)}$. On the contrary, if $d_g < 0$, then $v_g^{(2n+1)} > v_g^{(2n)}$. As a result, one can see that the pulse in Figs. 4(a) and 4(b) is slightly tilted towards the positive and negative part of the delay τ, respectively. These features are more visible in Figs. 4(c) and 4(d), where we show the pulse propagation in the central waveguide $n = 0$ (an example for even waveguides) when $d_g = 2$ and -2, respectively; and in Figs. 4(e) and 4(f), where we show the pulse propagation in the waveguide with position $n = 3$ (an example for odd waveguides) when $d_g = 2$ and -2, respectively. These features are understandable, because the reference frame (ξ, τ) used in Eqs. (4) and (5) moves with the speed which is equal to the group velocity $v_g^{(2n)} = 1/\beta_1^{(2n)}$ in even waveguides. So, when $d_g > 0$ (i.e., $v_g^{(2n+1)} < v_g^{(2n)}$) pulses in odd waveguides move slower than the reference frame. However, pulses in even and odd waveguides are coupled to each other as governed by Eqs. (4) and (5). As a result, when $d_g > 0$ coupled pulses in both even and odd waveguides propagate with group velocity smaller than $v_g^{(2n)}$ and the pulses in Figs. 4(a), 4(c), and 4(e) are slightly tilted towards the positive part of τ. On the contrary, when $d_g < 0$ coupled pulses in both even and odd waveguides propagate with group velocity greater than $v_g^{(2n)}$ and the pulses in Figs. 4(b), 4(d), and 4(f) are slightly tilted towards the negative part of τ. Note that pulses analyzed in Figs. 1, 2, and 3 are governed by Eq. (6), where all disturbing factors are neglected, thus they propagate with the group velocity $v_g^{(2n)}$ and must be symmetrical with respect to the central delay $\tau = 0$.

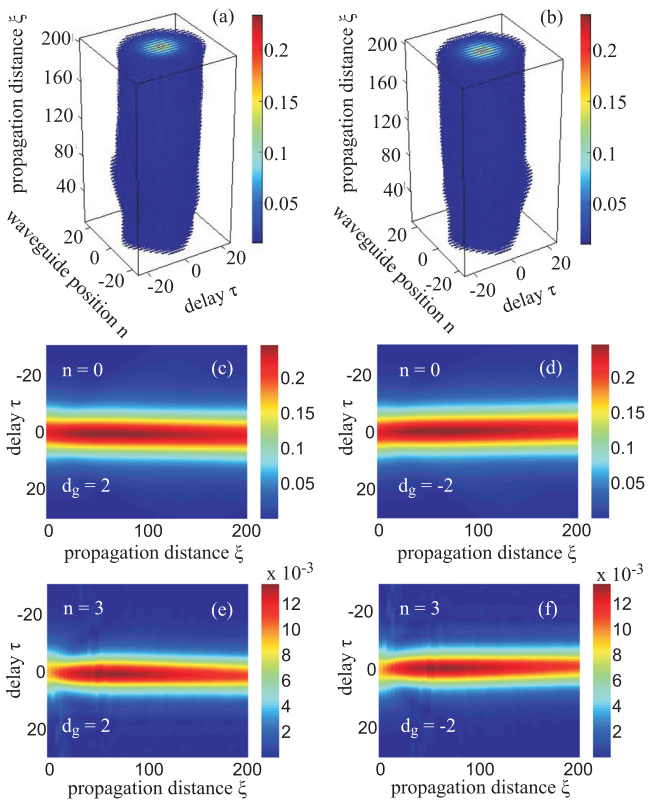

FIG. 4. (a) and (b) Evolution of a pulse in the (n,τ,ξ) space when $d_g = 2$ and -2, respectively. (c) and (d) Pulse propagation in the central waveguide $n = 0$ when $d_g = 2$ and -2, respectively. (e) and (f) The same as (c) and (d), but now in the waveguide with $n = 3$. All other parameters are the same as in Fig. 1.

Now, we investigate the influence of the GVD difference between adjacent waveguides represented by the parameter d_2. In Figs. 5(a) and 5(b), we show the evolution of the DLB investigated in Figs. 1 and 2, but now $d_2 = 1.5$ and -1.5, respectively. In the case $d_2 = 1.5$, both even and odd waveguides operate in the anomalous dispersion regime in which bright temporal solitons can be formed.[63] In this case, as shown in Fig. 5(a), the influence of the GVD difference between adjacent waveguides is quite slight, and the dynamics of the DLB in Figs. 5(a) and 1(a) is practically the same. This is understandable, because the fields in odd waveguides are much weaker than the fields in even waveguides [see Fig. 2(d)], therefore the contribution of the fields in odd waveguides in the dynamics of the DLB is not significant. However, in Fig. 5(b) the parameter $d_2 = -1.5$, so we have the anomalous dispersion regime in even waveguides, but the normal dispersion regime in odd waveguides. Because the temporal bright soliton is not supported now in odd waveguides, thus, the conditions are now not favorable for LBD formation in BWAs. As a result, there is a much more significant distortion of the pulse in Fig. 5(b) as compared to Fig. 1(a). It is worth mentioning that in practical situations, the absolute value of d_2 is much closer to unity. In this case, the GVD difference between adjacent waveguides in BWAs has just a minimal impact on the DLB dynamics.

In the rest of this work, we investigate the dynamics of DLBs in BWAs under the influence of the Raman effect. It is quite well known that the Raman effect is proportional to $1/T_p^4$ with T_p being the pulse duration.[66] As reported in Ref. 67, even with short pulses ($T_{FWHM} = 262$ fs), the Raman

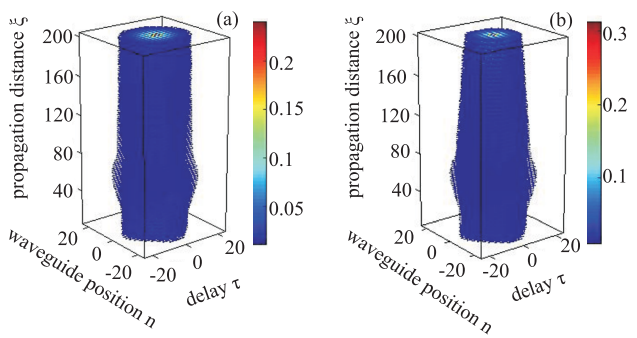

FIG. 5. (a) and (b) Evolution of a pulse in the (n,τ,ξ) space when $d_2 = 1.5$ and -1.5, respectively. All other parameters are the same as in Fig. 1.

effect plays just a minor role at the initial stage of the pulse propagation when the significant temporal compression has not occurred yet. It has a central role in pulse dynamics only after the significant temporal compression of the pulse. Therefore, it is expected that for the broad DLB illustrated in Fig. 1, the Raman effect is negligible [like the situation for the broad LB in WAs shown in Fig. 6(a) in Ref. 57]. Indeed, this is confirmed by our simulations (not shown here). As mentioned above, the Raman effect will be crucial if the significant temporal compression of the pulse takes place during propagation. This was dramatically demonstrated in Fig. 7 in Ref. 57 where the peak amplitude of the initial pulse is increased by just 6% as compared to the peak amplitude of the broad LB in WAs. However, for DLBs in BWAs it turns out that the Raman effect is not so crucial. In Fig. 6(a), we show the evolution of a pulse in the (n,τ,ξ) space when the Raman effect is taken into account, but without group velocity mismatch between adjacent waveguides ($d_g = 0$). The parameter $b_0 = 1.335$ in Fig. 6(a) is also larger by 6% as compared to the value $b_0 = 1.26$ in Fig. 1(a). So, the only difference in conditions between Figs. 6(a) and 3(b) is that in Fig. 6(a) the Raman effect is included, whereas it is excluded in Fig. 3(b). The Raman effect only bends the pulse in Fig. 6(a) at the moment of its compression towards the positive part of τ, i.e., the common de-acceleration of the pulse by the Raman effect.[63] This trend is more clearly illustrated in Fig. 6(c) where the pulse propagation in the central waveguide $n = 0$ is taken from Fig. 6(a). Before and after the compression in Figs. 6(a) and 6(c), the Raman effect is minimal because the pulse is large enough. So, with the same increase of 6% in the initial peak amplitudes of DLBs in BWAs and LBs in WAs, one can see that the Raman effect plays only a

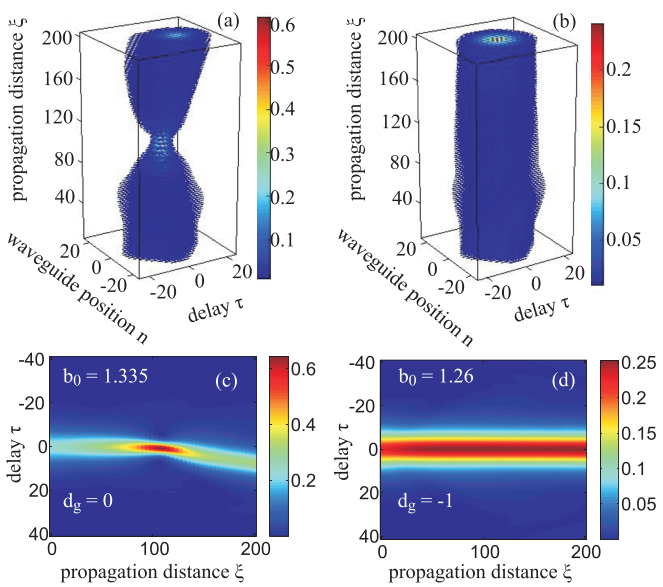

FIG. 6. (a) Evolution of a pulse in the (n,τ,ξ) space when the Raman effect is taken into account, but without group velocity mismatch between adjacent waveguides ($d_g = 0$), $b_0 = 1.335$. (b) Evolution of a pulse in the (n,τ,ξ) space when the Raman effect and group velocity mismatch between adjacent waveguides ($d_g = -1$) are both taken into account in the case $b_0 = 1.26$. (c) The pulse propagation in the central waveguide $n = 0$ and taken from (a). (d) Pulse propagation in the central waveguide $n = 0$ and taken from (b). All other parameters are the same as in Fig. 1.

mild effect on DLBs in BWAs as compared to a dramatic effect on LBs in WAs. This difference is due to the fact that when the initial peak amplitude is increased by 6%, the LBs in WAs are strongly compressed in both time and space, whereas the DLBs in BWAs are only mildly compressed. We conjecture that the binary nature of the system is again the root cause for the mild compression of DLBs in BWAs where a weak component (which, obviously, is very hard to be compressed) is coupled to a strong component. In order to compress the DLBs much more strongly, one needs to increase the peak amplitude of the initial pulse much further. In that case, like the situation with narrow light bullets in the presence of the Raman effect in uniform WAs demonstrated in Fig. 7 in Ref. 57, we expect that it is possible to form intense light bullets localized just in few waveguides of BWAs which are also short in the time domain.

In Figs. 4(b), 4(d), and 4(f), we have shown that when the group velocity mismatch parameter d_g is negative, the pulse can be bent towards the negative part of delay τ. At the same time, we have just shown in Figs. 6(a) and 6(c) that the Raman effect can bend the pulse towards the positive part of τ. So, in some circumstances these effects can compensate each other and help to stabilize the DLBs if they are included at the same time. This is illustrated in Figs. 6(b) and 6(d) where we show the evolution of the DLB in the (n,τ,ξ) space and in the central waveguide $n = 0$, respectively. This DLB has already been shown in Fig. 1 without the Raman effect, but now both these two above-mentioned effects are included. As clearly seen in Figs. 6(b) and 6(d), the DLB is quite well stabilized along the central delay axis ($\tau = 0$). For parameters used in Figs. 6(b) and 6(d), $d_g = -1$ is enough to compensate the Raman effect. If $d_g < -1$ the pulse will be bent towards the negative part of τ, whereas if $d_g > -1$, the pulse will be bent towards the positive part of τ.

Regarding the excitation of gap solitons both in fiber Bragg gratings and BWAs, there is a well-known problem due to the strong reflection.[20] Another approach has been proposed in Ref. 26 to avoid this problem. This approach is based on the fact that the odd components a_{2n-1} of the Dirac soliton are much weaker than its even components. At the very input, one can excite just even waveguides of BWAs by realizing some spatial delay Δz inside the sample for odd waveguides [see this scheme in Fig. 3(f) in Ref. 26]. The simulation results in Fig. 3 in Ref. 26 show that after some propagation distance the weak components in odd waveguides will be generated and the right profile of Dirac solitons will be formed during propagation. We believe that this approach can also increase the excitation efficiency for Dirac light bullets in BWAs. For the final note, we think that it is possible to realize the Klein tunneling of Dirac solitons and Dirac light bullets by using, for instance, the scheme of BWAs proposed in Ref. 14. This interesting topic will be covered elsewhere.

V. CONCLUSIONS

In conclusion, we have numerically demonstrated that in BWAs made of material with Kerr-type nonlinearity, broad

DLBs can be established during propagation of pulses, even if its input profiles are slightly different from the ones of established DLBs. The binary nature of the system, which leads to the fact that the intense and weak components of DLBs located at adjacent waveguides are always coupled to each other, helps decrease the influence of disturbing factors such as group velocity mismatch, GVD difference between adjacent waveguides, and the Raman effect. As a result, the DLBs can robustly propagate for hundreds of dispersion lengths in BWAs. With typical parameters for BWAs, the group velocity mismatch can only slightly accelerate or decelerate the DLBs, whereas the GVD difference between adjacent waveguides plays just a minor role in DLBs dynamics if all of its components operate in the anomalous dispersion regime. The Raman effect also plays only a negligible role in the dynamics of broad DLBs. We expect that DLBs can potentially have various applications in science and technology in the future.

ACKNOWLEDGMENTS

This research was funded by the Vietnam National Foundation for Science and Technology Development (NAFOSTED) under Grant No. 103.03-2016.01.

[1]D. N. Christodoulides, F. Lederer, and Y. Silberberg, Nature **424**, 817–823 (2003).
[2]A. L. Jones, J. Opt. Soc. Am. **55**, 261–269 (1965).
[3]D. N. Christodoulides and R. I. Joseph, Opt. Lett. **13**, 794–796 (1988).
[4]Y. S. Kivshar and G. P. Agrawal, *Optical Solitons: From Fibers to Photonic Crystals* (Academic Press, 2003).
[5]D. N. Christodoulides and E. D. Eugenieva, Phys. Rev. Lett. **87**, 233901 (2001).
[6]T. X. Tran and F. Biancalana, Phys. Rev. Lett. **110**, 113903 (2013).
[7]T. X. Tran and F. Biancalana, Opt. Express **21**, 17539–17546 (2013).
[8]T. X. Tran, D. C. Duong, and F. Biancalana, Phys. Rev. A **89**, 013826 (2014).
[9]F. Lederer, G. I. Stegeman, D. N. Christodoulides, G. Assanto, M. Segev, and Y. Silberberg, Phys. Rep. **463**, 1–126 (2008).
[10]T. Pertsch, P. Dannberg, W. Elflein, A. Bräuer, and F. Lederer, Phys. Rev. Lett. **83**, 4752 (1999).
[11]M. Ghulinyan, C. J. Oton, Z. Gaburro, L. Pavesi, C. Toninelli, and D. S. Wiersma, Phys. Rev. Lett. **94**, 127401 (2005).
[12]H. Trompeter, T. Pertsch, F. Lederer, D. Michaelis, U. Streppel, A. Bräuer, and U. Peschel, Phys. Rev. Lett. **96**, 023901 (2006).
[13]S. Longhi, Phys. Rev. B **81**, 075102 (2010).
[14]F. Dreisow, R. Keil, A. Tünnermann, S. Nolte, S. Longhi, and A. Szameit, Europhys. Lett. **97**, 10008 (2012).
[15]S. Longhi, Opt. Lett. **35**, 235–237 (2010).
[16]F. Dreisow, M. Heinrich, R. Keil, A. Tünnermann, S. Nolte, S. Longhi, and A. Szameit, Phys. Rev. Lett. **105**, 143902 (2010).
[17]S. Longhi, Appl. Phys. B **104**, 453–468 (2011).
[18]J. M. Zeuner, N. K. Efremidis, R. Keil, F. Dreisow, D. N. Christodoulides, A. Tünnermann, S. Nolte, and A. Szameit, Phys. Rev. Lett. **109**, 023602 (2012).
[19]A. A. Sukhorukov and Y. S. Kivshar, Opt. Lett. **27**, 2112–2114 (2002).
[20]A. A. Sukhorukov and Y. S. Kivshar, Opt. Lett. **28**, 2345–2347 (2003).
[21]M. Conforti, C. De Angelis, and T. R. Akylas, Phys. Rev. A **83**, 043822 (2011).
[22]R. Morandotti, D. Mandelik, Y. Silberberg, J. S. Aitchison, M. Sorel, D. N. Christodoulides, A. A. Sukhorukov, and Y. S. Kivshar, Opt. Lett. **29**, 2890–2892 (2004).
[23]M. Johansson, K. Kirr, A. S. Kovalev, and L. Kroon, Phys. Scr. **83**, 065005 (2011).
[24]A. Gorbach and M. Johansson, Eur. Phys. J. D **29**, 77–93 (2004).
[25]Y. S. Kivshar and N. Flytzanis, Phys. Rev. A **46**, 7972 (1992).
[26]T. X. Tran, S. Longhi, and F. Biancalana, Ann. Phys. **340**, 179–187 (2014).
[27]T. X. Tran, X. N. Nguyen, and D. C. Duong, J. Opt. Soc. Am. B **31**, 1132–1136 (2014).
[28]T. X. Tran, X. N. Nguyen, and F. Biancalana, Phys. Rev. A **91**, 023814 (2015).
[29]T. X. Tran and D. C. Duong, Ann. Phys. **361**, 501–508 (2015).
[30]W. Heisenberg, Rev. Mod. Phys. **29**, 269–278 (1957).
[31]D. C. Ionescu, J. Reinhardt, B. Muller, W. Greiner, and G. Soff, Phys. Rev. A **38**, 616 (1988).
[32]A. Zecca, Int. J. Theor. Phys. **41**, 421–428 (2002).
[33]M. J. Esteban and E. Séré, Discrete Contin. Dyn. Syst. **8**, 381–397 (2002).
[34]I. Bialynicki-Birula and J. Mycielski, Ann. Phys. **100**, 62–93 (1976).
[35]W. Chen and D. L. Mills, Phys. Rev. Lett. **58**, 160–163 (1987).
[36]D. N. Christodoulides and R. I. Joseph, Phys. Rev. Lett. **62**, 1746–1749 (1989).
[37]A. B. Aceves and S. Wabnitz, Phys. Lett. A **141**, 37–42 (1989).
[38]W. E. Thirring, Ann. Phys. **3**, 91–112 (1958).
[39]C. M. de Sterke and J. E. Sipe, Phys. Rev. A **42**, 550–555 (1990).
[40]C. Conti and S. Trillo, Phys. Rev. E **64**, 036617 (2001).
[41]I. V. Barashenkov, D. E. Pelinovsky, and E. V. Zemlyanaya, Phys. Rev. Lett. **80**, 5117–5120 (1998).
[42]A. De Rossi, C. Conti, and S. Trillo, Phys. Rev. Lett. **81**, 85–88 (1998).
[43]B. J. Eggleton, R. E. Slusher, C. M. de Sterke, P. A. Krug, and J. E. Sipe, Phys. Rev. Lett. **76**, 1627–1630 (1996).
[44]A. B. Aceves, Chaos **10**, 584–589 (2000).
[45]Y. Silberberg, Opt. Lett. **15**, 1282–1284 (1990).
[46]B. A. Malomed, D. Mihalache, F. Wise, and L. Torner, J. Opt. B: Quantum Semiclassical Opt. **7**, R53–R72 (2005).
[47]A. B. Aceves, C. De Angelis, A. M. Rubenchik, and S. K. Turitsyn, Opt. Lett. **19**, 329–331 (1994).
[48]A. B. Aceves, G. G. Luther, C. D. Angelis, A. M. Rubenchik, and S. K. Turitsyn, Phys. Rev. Lett. **75**, 73 (1995).
[49]E. W. Laedke, K. H. Spatschek, S. K. Turitsyn, and V. K. Mezentsev, Phys. Rev. E **52**, 5549 (1995).
[50]A. V. Buryak and N. N. Akhmediev, IEEE J. Quantum Electron. **31**, 682–688 (1995).
[51]X. Liu, L. J. Qian, and F. W. Wise, Phys. Rev. Lett. **82**, 4631 (1999).
[52]H. S. Eisenberg, R. Morandotti, Y. Silberberg, S. Bar-Ad, D. Ross, and J. S. Aitchison, Phys. Rev. Lett. **87**, 043902 (2001).
[53]D. Cheskis, S. Bar-Ad, R. Morandotti, J. S. Aitchison, H. S. Eisenberg, Y. Silberberg, and D. Ross, Phys. Rev. Lett. **91**, 223901 (2003).
[54]N. N. Rosanov, *Spatial Hysteresis and Optical Patterns* (Springer, 2002).
[55]N. N. Rosanov, in *Dissipative Solitons*, edited by N. Akhmediev and A. Ankiewicz (Springer-Verlag, 2005).
[56]N. N. Rosanov and T. X. Tran, Chaos **17**, 037114 (2007).
[57]T. X. Tran, D. C. Duong, and F. Biancalana, Phys. Rev. A **90**, 023857 (2014).
[58]A. B. Aceves, G. Fibich, and B. Ilan, Phys. D **189**, 277–286 (2004).
[59]T. Dohnal and A. B. Aceves, Stud. Appl. Math. **115**, 209–232 (2005).
[60]A. Sukhorukov and Y. S. Kivshar, Phys. Rev. Lett. **97**, 233901 (2006).
[61]N. Aközbek and S. John, Phys. Rev. E **57**, 2287–2319 (1998).
[62]G. P. Agrawal, *Applications of Nonlinear Fiber Optics*, 2nd. (Academic Press, 2008).
[63]G. P. Agrawal, *Nonlinear Fiber Optics*, 5th ed. (Academic Press, 2013).
[64]S. Longhi, Phys. Res. Int. **2010**, 645106 (2010).
[65]D. Mandelik, H. S. Eisenberg, Y. Silberberg, R. Morandotti, and J. S. Aitchison, Phys. Rev. Lett. **90**, 053902 (2003).
[66]J. P. Gordon, Opt. Lett. **11**, 662–664 (1986).
[67]T. X. Tran and F. Biancalana, Phys. Rev. A **79**, 065802 (2009).